Preparation and Characterization of Magnetic Nanofibers with Iron Oxide Nanoparticles and Poly(ethylene terephthalate)

Byung Wook Ahn, Tae Jin Kang

Department of Materials Science and Engineering, Seoul National University, Deahak-dong, Gwanak-gu, Seoul 151-742, Korea

Received 15 October 2010; accepted 22 May 2011
DOI 10.1002/app.34953
Published online 16 January 2012 in Wiley Online Library (wileyonlinelibrary.com).

ABSTRACT: Iron oxide nanoparticle/Poly(ethylene terephthalate) (PET) nanowebs were obtained by electrospinning. To achieve superparamagnetic properties, iron oxide nanoparticles with diameters below 25 nm were used. Diameter distribution of iron oxide nanoparticles was measured by a particle size analyzer. Iron oxide nanoparticles were added into 16 wt % PET solution in the ratio of 5, 10, and 15 wt % to PET. The morphology of iron oxide nanoparticle/PET nanowebs was observed using field emission-scanning electron microscopy (FE-SEM) and transmission electron microscopy (TEM). The nanofiber diameter increased as increasing iron oxide nanoparticle concentration. The superparamagnetic behavior of iron oxide nanoparticle/PET nanofiber was confirmed using superconducting quantum interference device (SQUID). The degree of crystallinity of iron oxide nanoparticle/PET nanowebs was calculated from a differential scanning calorimeter (DSC) results. The change of flexural rigidity and tensile properties of electrospun iron oxide nanoparticle/PET nanowebs with the external magnetic field were examined ISO 9073-7 testing method, universal testing machine and an appropriate magnet. Also, the elastic modulus of iron oxide nanoparticle/PET nanofiber was measured using nanoindentation. With applying magnetic field, the improvement in mechanical properties of field-responsive magnetic nanofibers and nanowebs was confirmed.
 J Appl Polym Sci 125: 1567–1575, 2012

Key words: nanofiber; magnetic polymers; mechanical properties; polyesters; crystallization

INTRODUCTION

Magnetic fibers have attracted many researchers' attention due to its various potential applications as magnetic filters, sensors, drug delivery system, and electromagnetic devices for information storage.[1–5] Till now, various types of magnetic nanofibers including pure ferromagnetic metal fibers, polymeric fibers that are blended or coated with magnetic particles and magnetic fibers with the core/sheath structure were introduced.[6–9] Each type has both several advantages and disadvantage, so it is needed to design the type of magnetic nanofibers suited for a certain application.

It is well known that the ferromagnetic materials such as iron oxide no longer maintain their intrinsic ferromagnetism as the material size decreases to dozens nanometer.[10] When the size of magnetic domain decreases, the effect of thermal fluctuation becomes not negligible.[11,12] Consequently, the remnant magnetization at zero field decreases and the relaxation of magnetic dipole moments becomes more reversible and fast. The materials with this superparamagnetic behavior can be applied to field-responsive protection due to its reversible and fast fortification caused by the alignment of magnetic particles. Especially, in the case that the flexibility of the material is required in time of no emergency, the combination with flexible polymeric nanofiber can be good choice.

There are several methods to obtain microfibers or nanofibers. Commonly used methods include template synthesis,[13] phase separation,[14] self-assembly,[15] electrospinning,[16,17] etc. Electrospinning is an easy method to produce nanofibers using simple equipment. Recently, electrospinning with two and more materials has been used to obtain nanowebs, which have excellent properties.[18–22]

In this study, we fabricated the superparamagnetic nanofibers of blend type by electrospinning with iron oxide nanoparticles and Poly(ethylene terephthalate) (PET), an important commercial thermoplastic polymer. The morphology, crystallinity, and magnetic behavior of the nanofibers were examined and the several mechanical properties were tested with magnetic field generators to explore the potential for application of magnetic nanofibers to field-responsive protection.

EXPERIMENTAL

Materials and preparation of electrospinning dope

Iron oxide nanoparticles (Fe_3O_4, <50 nm, >98% trace metals basis) were purchased from Aldrich, USA. PET bright chips (M_w 19,200) were supplied by

Correspondence to: T. J. Kang (taekang@snu.ac.kr).

Toray-Saehan, Korea. Trifluoroacetic acid (TFA, 99%) was obtained from Samchun chemicals, Korea.

First, iron oxide nanoparticles with sizes below 25 nm were separated. Iron oxide nanoparticles in ethanol were bath-sonicated for 30 min and 70–80% supernatant was extracted and dried in an oven to evaporate ethanol. The particle size distribution of the extracted iron oxide nanoparticles was measured by a particle size analyzer (Nanotrac ultra, Microtrac, US). PET chips were dissolved in TFA to obtain 16 wt % solution. Afterward, iron oxide nanoparticles were added into the PET solution and the mixture was bath-sonicated for 12 h. And just before electrospinning, the mixture was tip-sonicated for 5 min to avoid sedimentation of iron oxide nanoparticles. In this way, iron oxide nanoparticle/PET dopes were prepared with iron oxide nanoparticles concentrations of 5, 10, and 15 wt % to PET. For comparison, neat PET dope was also prepared.

Electrospinning

The morphology of electrospun nanofiber can be controlled by several electrospinning parameters and dope concentration. We used the following electrospinning conditions. The prepared dopes were electrospun using a robotic electrospinning system (NNC-ESP200R2, NanoNC, Korea). The applied voltage was 15 kV, and tip-to-collector distance was 15 cm. The inner diameter of the metal syringe tip was 0.686 mm. A moving aluminum plate was used as the collector to obtain nanowebs of even thickness. For nanoindentation test, the nanofibers were also collected on a Si wafer. Electrospinning dope was pushed out using a syringe pump (No. 200, KdScientific, US) at a rate of 1.5 mL/h. The syringe tip was located in the horizontal direction of the collector. For even thickness of nanoweb samples, 3 g of PET was electrospun in all cases. The electrospun nanofibers were dried in the vacuum oven for 3 days to completely evaporate TFA.

Characterization

The morphology of electrospun nanofibers was observed with a field emission-scanning electron microscope (FE-SEM JSM-6330F, JEOL, Japan). The distribution of nanofiber diameter was measured using a built-in counting program. High-resolution transmission electron microscope (HR-TEM JEM-3000F, JEOL, Japan) was used to observe the size and alignment of iron oxide nanoparticles in PET nanofibers with an accelerating voltage of 300 kV.

Calorimetric measurements were performed to examine the changes in crystallinity caused by iron oxide nanoparticle addition using a differential scanning calorimeter (DSC Q1000, TA Instrument, UK). The samples were heated from 40 to 300°C at a heating rate of 5°C/min under nitrogen atmosphere. The degree of crystallinity was calculated by the following equation:

$$\chi = \frac{\Delta H_f - \Delta H_c}{(1 - M_{Fe_3O_4})\Delta H_f^\circ} \times 100\%,$$

where, χ is the degree of crystallinity of iron oxide nanoparticle/PET nanoweb, M_{Fe_3O4} is the concentration of iron oxide nanoparticle, ΔH_f is the measured heat of melting, ΔH_c is the measured heat of cold crystallization, ΔH_f^o is the heat of fusion of 100% crystalline PET. ΔH_f^o was set as 140.1 J/g.[23]

The magnetic behavior was measured using the superconducting quantum interference device (SQUID, MPMS XL5, Quantum design). The magnetic field intensity ranged from −3,000 to +3,000 Oe and the measuring temperature was 300 K.

Flexural rigidity of electrospun nanoweb was measured. The change of flexural rigidity was observed when the external magnetic field was applied using a neodymium magnet. The test method was referred to ISO 9073-7. The experimental schematic was shown in Figure 1. Flexural rigidity was calculated by the following equation.

$$G = m \times C^3 \times 10^{-3},$$

where, G is the flexural rigidity (mN cm), m is weight per unit area (g/m^2), C is the bending length (cm).

Tensile properties were tested using a universal testing machine (Instron 5543). Tensile tests were performed with specimen size of 15 mm (gap) × 10 mm (width) × ~ 0.3 mm (thickness). We used the solenoid electromagnet to apply the uniform field gradient. The magnetic field intensity of the inside of the solenoid was about 0.1 T. The specimens were

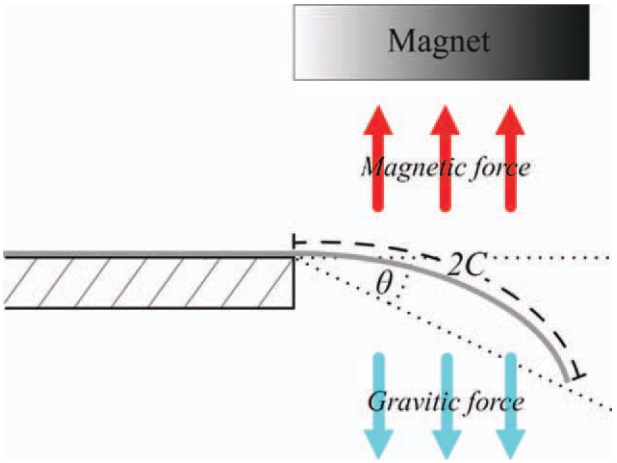

Figure 1 A schematic diagram of flexural rigidity measurement. [Color figure can be viewed in the online issue, which is available at wileyonlinelibrary.com.]

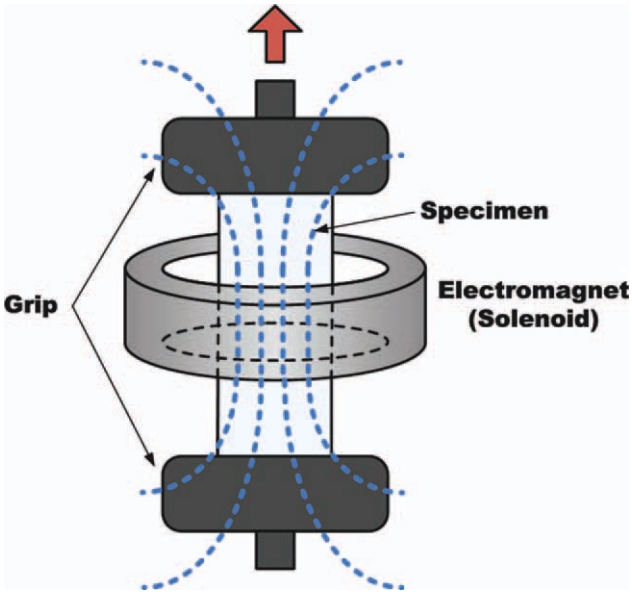

Figure 2 A schematic diagram of tensile test with an electromagnet. [Color figure can be viewed in the online issue, which is available at wileyonlinelibrary.com.]

located in the midst of the solenoid electromagnet. The extension speed was 10 mm/min. The apparatus setting was illustrated in Figure 2.

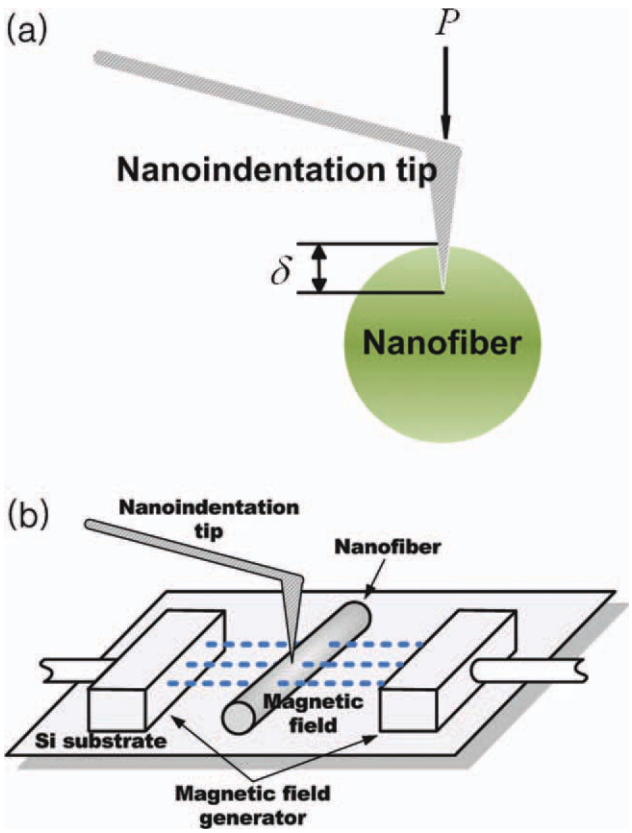

Figure 3 Schematic diagrams of (a) nanoindentation test and (b) nanoindentation test with a magnetic field generator. [Color figure can be viewed in the online issue, which is available at wileyonlinelibrary.com.]

The elastic modulus of one nanofiber was measured by nanoindentation method (Fig. 3). A nanoindentation tip (pyramidal shape, Park system, Korea) and magnetic field generator (−0.03 – +0.03 T, Park system, Korea) were installed to atomic force microscope (AFM, XE-100, Park system, Korea). We observed the change in elastic modulus of one nanofiber when the external magnetic field was applied. The elastic modulus of nanofibers was calculated according to the following equations.[24] The relative elastic modulus E_r is given by

$$E_r = \sqrt{\frac{9P^2}{16R_e\delta^2}},$$

where, P is the applied force, δ is the indentation depth, and R_e is the equivalent radius for a indenter in contact. R_e is given by

$$R_e = \sqrt{\frac{R_t^2 R_f}{R_t + R_f}},$$

where, R_t is the indenter tip radius (25 nm) and R_f is the radius of the nanofiber. R_f was determined by analysis of the height profile using AFM. Every measurement was done with the nanofibers, which diameter was about 600 ± 50 nm. The elastic modulus of nanofiber E_f is given by

$$E_f \approx E_r(1 - \nu_f^2),$$

where, v_f is the Poisson's ratio of the nanofiber (0.33).

RESULTS AND DISCUSSION

Morphology

Figure 4 shows size distribution of iron oxide nanoparticles. The number average diameter was about

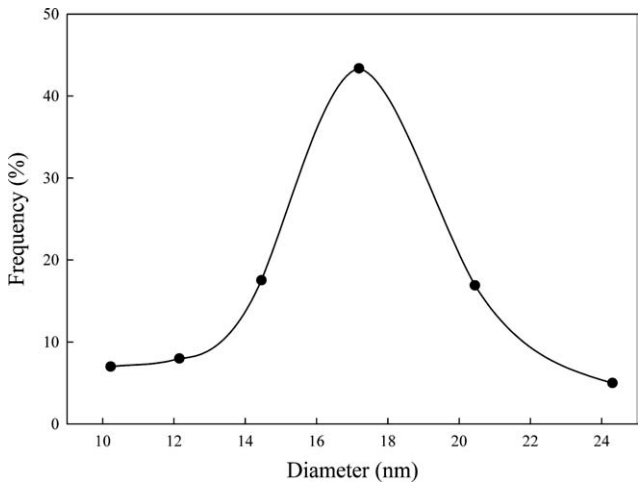

Figure 4 Diameter distribution of iron oxide nanoparticles.

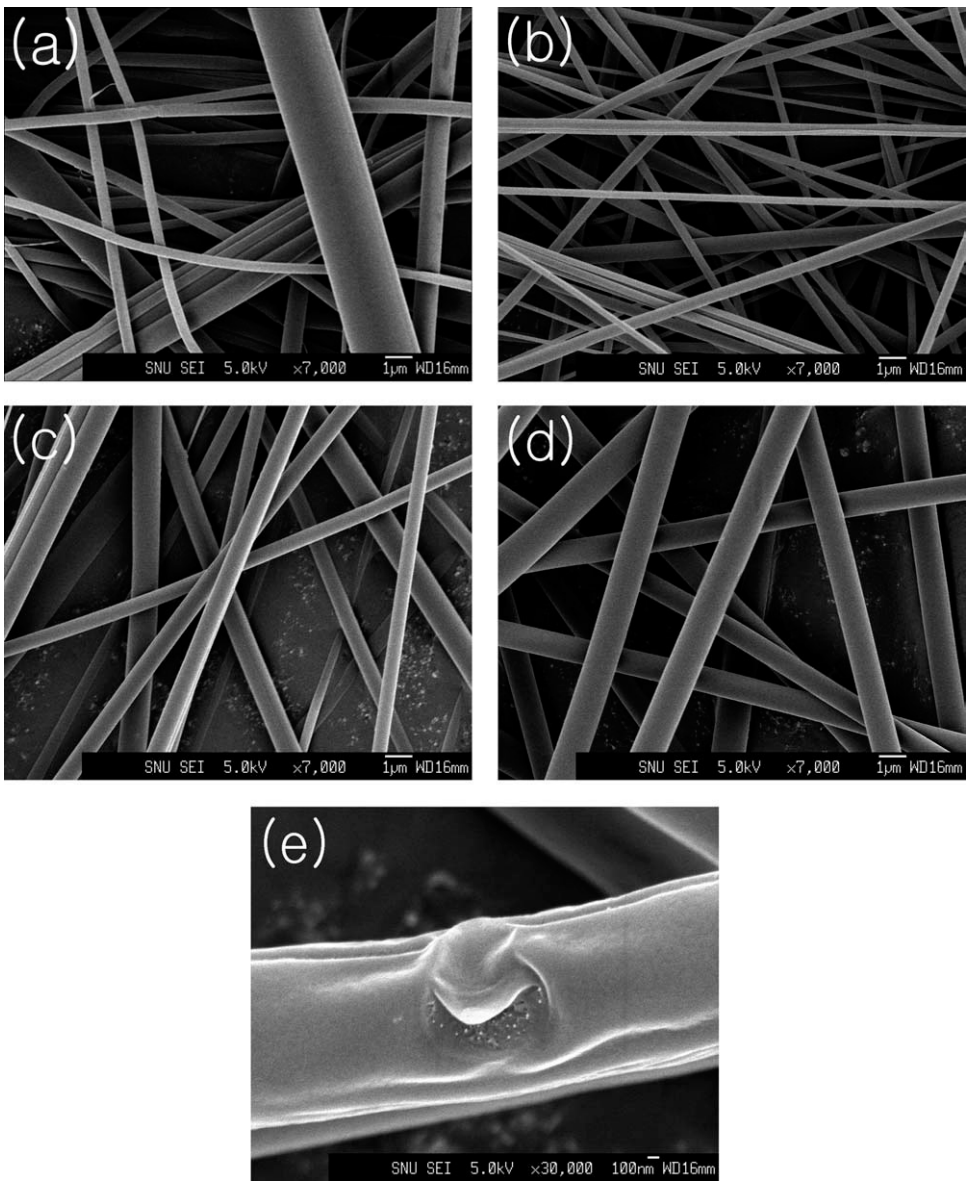

Figure 5 SEM photos of (a) neat PET nanofibers and iron oxide nanoparticle/PET nanofiber with the iron oxide nanoparticle concentrations of (b) 5 wt %, (c) 10 wt %, and (d) 15 wt %. (e) The exposed iron oxide nanoparticles at defected spot.

17 nm, small size enough to show the superparamagnetic behavior. Figures 5 and 6 show SEM photographs of iron oxide nanoparticle/PET nanofibers and diameter distribution of the nanofibers, respectively. The diameters of neat PET nanofibers show a broad distribution resulting from unstability of the electrospinning jet. However, relatively uniform distributions of the diameters were observed in the case of iron oxide nanoparticle/PET nanofibers. It seems that addition of charge carriers (iron oxide nanoparticles) into the electrospinning dope reduced unstability of the electrospinning jet. The average diameter of iron oxide nanoparticle/PET nanofibers increased with iron oxide nanoparticle concentration. Iron oxide nanoparticles that can act as charge carriers increase the Coulomb force acted on the electrospinning dope. As the attractive force between the electrospinning jet and the collector increases, the nanofibers experience a higher stretching force.[25] But it is also known that increase in dope viscosity causes the increase in the diameter of electrospun nanofibers.[26] Therefore, the competition between an electric charge(i.e., Coulomb force) and dope viscosity(i.e., cohesiveness) affects the diameter of electrospun nanofibers. Thus, rheological analysis was done to know, which one among dope viscosity and Coulomb force mainly affected the diameter distribution of nanofibers (Fig. 7). Viscosity of 5 wt % iron oxide nanoparticle/PET solution was lower than that of neat PET solution at the lower shear

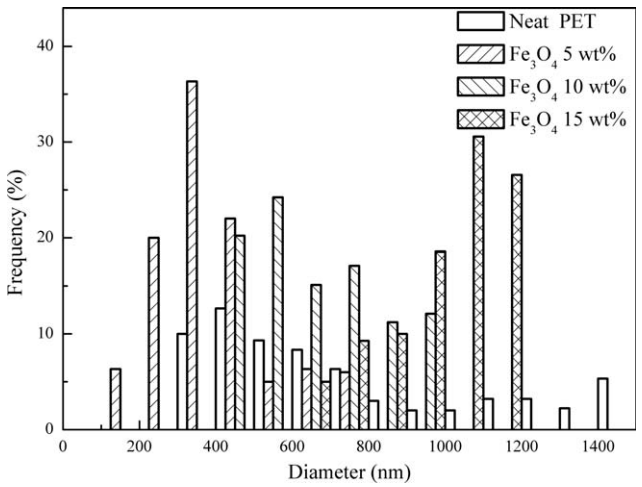

Figure 6 Diameter distributions of neat PET and iron oxide nanoparticle/PET nanofibers.

rate range. It is common phenomenon in the case of particle-dispersed polymer solutions.[27] Particles incorporated into the entanglement of polymer chains during stirring or sonication may help disentangle them, causing decrease of dope viscosity. The length of PET used in this work was about 100 nm (calculated from monomer length 10.75 Å [28]), which is large enough to allow particle incorporation. And because specific gravity of iron oxide nanoparticles (5.2[29]) is about four times higher than that of PET (1.4[23]), particle incorporation between polymer chains would be easy in dynamic environment. Also viscosity increase by iron oxide nanoparticles themselves was observed when iron oxide nanoparticle concentration increased from 5 to 15 wt %. It seems that viscosity increment by existence of iron oxide nanoparticles resulting in interparticle or particle–polymer interactions was lower than viscosity decrement by disentanglement of polymer chains in case of 5 wt % iron oxide nanoparticle/PET solution. And in case of 10 and 15 wt % iron oxide nanoparticle/PET solution, the former overwhelmed the latter. However, polymer chains might be disentangled enough with addition of just 5–10 wt % iron oxide nanoparticles. Viscosity of iron oxide nanoparticle/PET solution started to decrease as the shear rate became higher. Electrospinning is a process undertaken at high shear rate ($>10^3$ s^1). Iron oxide nanoparticles have a zero-dimensional structure, so it is difficult to expect a dramatic shear thinning effect, which can be easily shown in the case of the fluidal mixture including one dimensional structure material such as carbon nanotube. Actually, the shear thinning effect of iron oxide nanoparticle/PET solutions was weaker than that of neat PET solution. Consequently, the dope viscosity was proportional to the iron oxide content at higher shear rates. Thus, it is thought that the later factor (dope viscosity) preferred to the former factor (Coulomb force) in our experiments. As a result, the average diameter of iron oxide nanoparticle/PET nanofibers increased with iron oxide nanoparticle concentration.

Figure 8 shows the TEM images of iron oxide nanoparticle/PET nanofibers. Relatively uniform dispersion of iron oxide nanoparticles in PET nanofibers was confirmed. But, as iron oxide nanoparticles loading increases, aggregations of iron oxide nanoparticles tended to increase. Due to their high surface-to-volume ratio, magnetic nanoparticles tend to agglomerate each other for reducing own energy.

Differential scanning calorimetry result

DSC thermograms are shown in Figure 9. The degree of crystallinity χ, glass transition temperature T_g, cold crystallization temperature T_{cc} and melting temperature T_m are summarized in Table I. The glass transition temperature increased slightly with iron oxide nanoparticle concentration. The limited mobility of polymer chains by iron oxide nanoparticles might be responsible for that.[30] DSC measurements are progressed with solid samples in a static state. As a natural result, foreign substances like iron oxide nanoparticles can disturb movement of polymer chains to some extent. However, T_g of neat PET nanoweb was higher than 5 wt % iron oxide nanoparticle/PET nanoweb. This is might be due to the existence of less disentangled polymer chains in comparison with iron oxide nanoparticle/PET nanowebs. T_{cc} and the onset temperature of cold crystallization moved to a higher temperature and the degree of crystallinity increased with iron oxide nanoparticle loading, indicating that hard metal particles such as iron oxide nanoparticles does not assist heat-induced crystallization but play a helpful role in crystallization of PET during electrospinning process. The disentanglement of polymer chains during crystallization is closely related to the

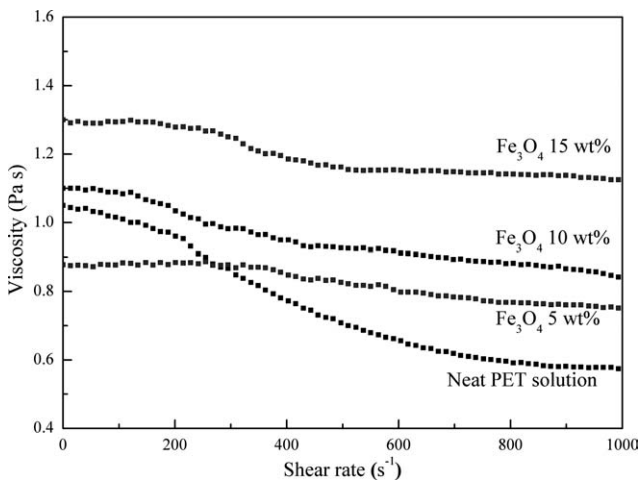

Figure 7 Plot of viscosity versus shear rate for neat PET and iron oxide nanoparticle/PET dopes.

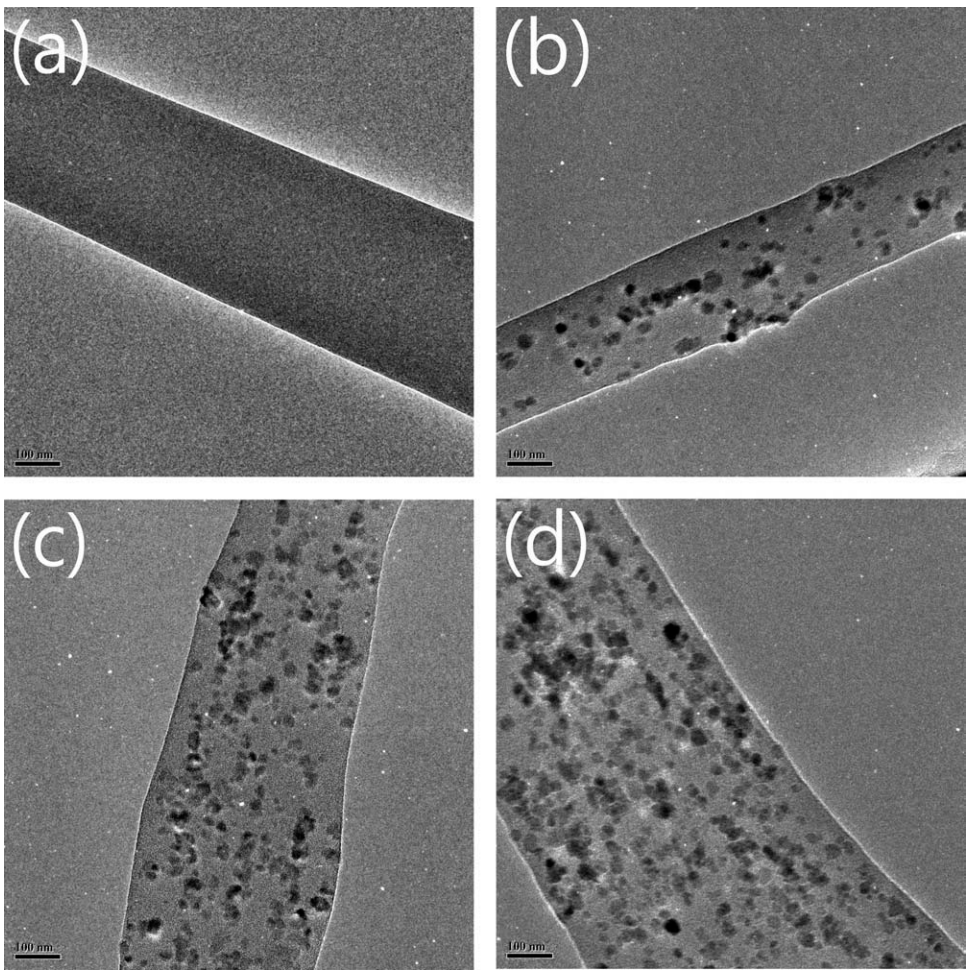

Figure 8 HR-TEM images of (a) a neat PET nanofiber and iron oxide nanoparticle/PET nanofibers with the iron oxide nanoparticle concentrations of (b) 5 wt %, (c) 10 wt %, and (d) 15 wt %.

degree of crystallinity.[31] The disentanglement of polymer chain by iron oxide nanoparticles during electrospinning process is assumed to be responsible for increased crystallinity. There was not a significant difference between the crystallinity of 10 and 15 wt % iron oxide nanoparticle/PET nanowebs. The disentanglement of a similar extent in two samples as assumed in the rheological analysis is thought to be responsible for that.

The crystallinity of electrospun nanowebs was lower than that of conventional PET films or yarns due to absence of the annealing process and relatively little time for crystallization.[32]

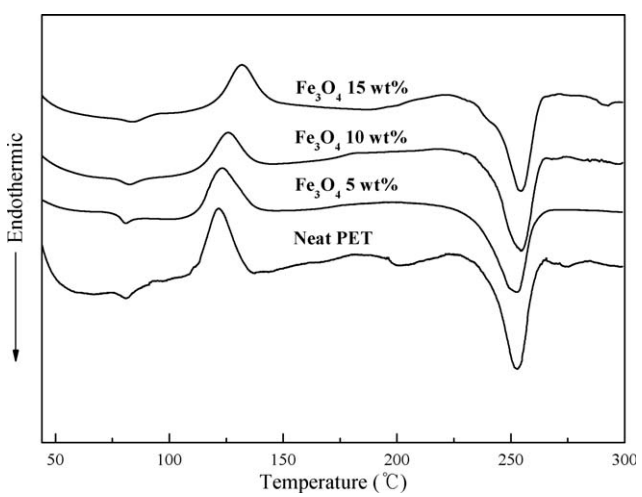

Figure 9 DSC thermograms of neat PET and iron oxide nanoparticle/PET nanowebs.

Magnetic curve

Figure 10 shows the magnetic curves of the iron oxide nanoparticle/PET nanofibers. The magnetic

TABLE I
DSC Results of Neat PET and Iron Oxide Nanoparticle/PET Nanowebs

	T_g (°C)	T_{cc} (°C)	T_m (°C)	χ (%)
Neat PET	81.3	121.8	252.8	12.06
5 wt % Fe_3O_4	80.8	123.0	252.9	16.42
10 wt % Fe_3O_4	82.4	125.9	254.3	18.86
15 wt % Fe_3O_4	84.2	131.8	254.6	18.60

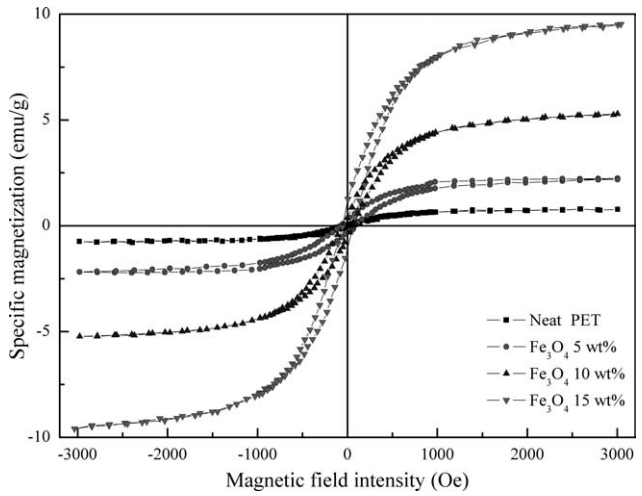

Figure 10 Magnetic curves of iron oxide nanoparticle/PET nanofibers.

curves show a narrow hysteresis and a small remnant magnetization at zero field. This near-superparamagnetism is well known to be related with the fast magnetic relaxation of the iron oxide nanoparticles.[10] This fast relaxation is caused by the removal of the polarization of the dipole moments of the nanoparticles due to the thermal fluctuation. However, the nanoparticles were arrested in the solid polymer matrix, thus the effect of the thermal fluctuation was not fully affected. And with increasing iron oxide nanoparticle concentration, the aggregations of iron oxide nanoparticles increased. So the magnetic domain size increased in some spots, the ferromagnetic behavior arose as a result. The remnant magnetization at zero field increased proportionally with iron oxide nanoparticle concentration (5 wt % → 0.3056 emu/g; 10 wt % → 0.3889 emu/g; 15 wt % → 1.1389 emu/g). The saturation magnetization was 2.23, 5.24, and 9.48 emu/g, respectively. Relatively smaller value of saturation magnetization than that of bulk iron is known to be general for magnetic nanomaterials.[33] Also, the confinement of magnetic nanoparticles in a solid polymer matrix might be responsible for that.

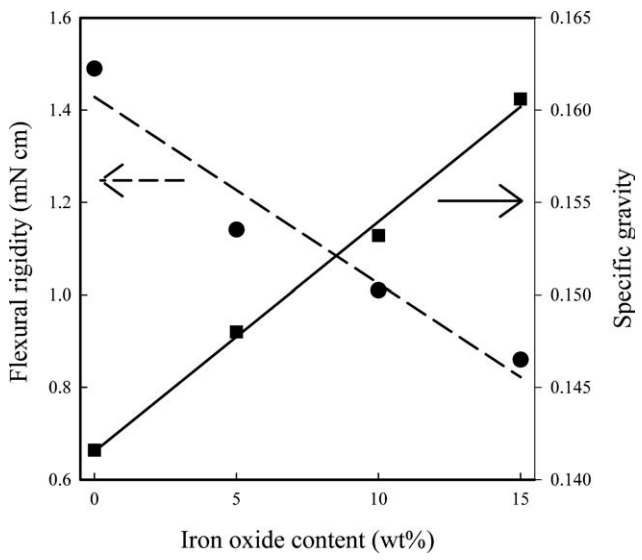

Figure 11 Specific gravity and flexural rigidity of iron oxide nanoparticle/PET nanowebs with no magnetic field.

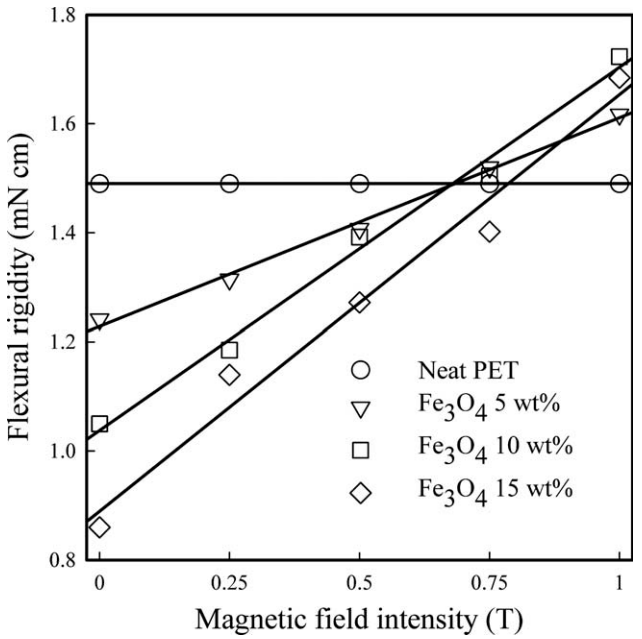

Figure 12 Flexural rigidity versus magnetic field intensity of neat PET and iron oxide nanoparticle/PET nanowebs with magnetic field.

Mechanical properties

Flexural rigidity

Flexural rigidity of the nanoweb is mainly affected by the specific gravity and modulus. The measured specific gravity and flexural rigidity of iron oxide nanoparticle/PET nanoweb are shown in Figure 11. As a natural result, specific gravity increased with increasing iron oxide nanoparticle concentration. And flexural rigidity of the nanoweb was inversely related to the specific gravity. When the external magnetic field was applied, flexural rigidity of iron oxide nanoparticle/PET nanowebs increased with help of the magnetic force (Fig. 12). As the magnetic field intensity increased, flexural rigidity increased. Also, the slope of graph was increased exactly with increasing iron oxide nanoparticle concentration. This increase of flexural rigidity with the external magnetic field is not result of the change in the intrinsic properties of the nanowebs. But it is thought that this test can be used as the one of the quantitative expression of the field-responsive relation between the magnetic field intensity and the magnetic material content of nanowebs or cloths.

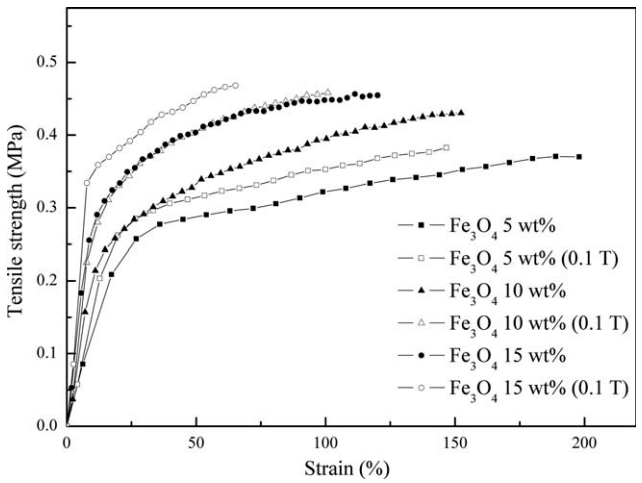

Figure 13 Stress-strain curves of iron oxide nanoparticle/PET nanowebs.

Tensile strength

Stress-strain curves of iron oxide nanoparticle/PET nanowebs are shown in Figure 13. The tensile strength of the nanowebs was lower than that of general PET films[34] or fibers.[35] Absence of post-processing such as annealing, weak bonding at nanofiber crossovers and the porous structure are responsible for the low tensile strength of nanowebs.[36] The rigid particles of low aspect ratio and small size (less than 5 μm) can act as toughenners in polymer matrix because the debonding energy between particles and matrix can contribute to increase of yield stress.[37] As a result, the tensile strength and modulus increased with increasing iron oxide nanoparticle concentration. Also, the increase of crystallinity and diameter with iron oxide nanoparticle loading could contribute to tensile toughening. However, upon 15 wt % iron oxide nanoparticle addition, enhancing effect of tensile strength and modulus decreased a little. It is thought that aggregations which are detrimental to particle toughening effect are responsible for that. Elongation at break decreased from 197 to 120% as iron oxide nanoparticle concentration reached 15 wt %. Stress concentration of rigid particles in polymer matrix increases with increasing volume fraction and aggregations.[38] It is assumed that increase of local failure due to stress concentrators resulted in strain decrease.

When an external magnetic field was applied, the iron oxide nanoparticle/PET nanowebs showed increased tensile strength and modulus, but reduced strain. A dipole-dipole interaction arises between the magnetic nanoparticles when the magnetic nanofiber is exposed to a magnetic field and the tensile axis component of such dipole-dipole interactions can act as a resistance force against the tensile stress. As the dipole-dipole interaction is inversely proportional to the square of distance between the magnetic nanoparticles,[39] this reinforcement effect of iron oxide nanoparticles under a magnetic field is more prominent in the initial stage of tensile deformation. Consequently, further improvement was observed in modulus values than tensile strength values. As tensile deformation progresses, the distance between the iron oxide nanoparticles increases along the tensile axis but decreases in the direction perpendicular to the tensile axis. Upon further tensile deformation, the distance between the magnetic nanoparticles perpendicular to the tensile axis become close enough to form aggregations due to the dipole-dipole interaction. Such aggregations act as stress concentrators, decreasing the strain. The tensile test results are listed in Table II.

TABLE II
Tensile Properties of Iron Oxide Nanoparticle/PET Nanowebs

	Tensile strength (MPa)	Elongation at break (%)	Modulus (MPa)
5 wt % Fe_3O_4	0.369	197	1.20
10 wt % Fe_3O_4	0.430	152	2.21
15 wt % Fe_3O_4	0.454	120	3.28
5 wt % Fe_3O_4 (0.1 T)	0.382	146	1.59
10 wt % Fe_3O_4 (0.1 T)	0.458	101	2.92
15 wt % Fe_3O_4 (0.1 T)	0.468	65	4.28

Nanoindentation

Figure 14 shows the nanoindentation curves of the iron oxide nanoparticle/PET nanofiber. From the specimen data and the reference (Si wafer) data, the load versus indentation depth curves were extracted. And the calculated elastic moduli are listed in Table III. As increasing the iron oxide nanoparticle concentration, the elastic modulus increased. This result is

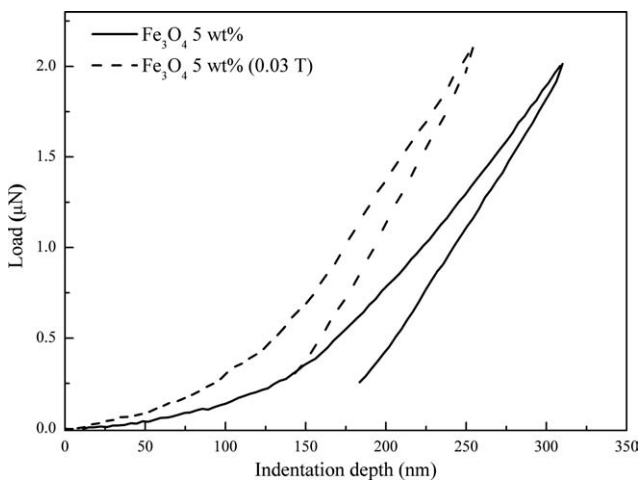

Figure 14 Nanoindentation curves of iron oxide nanoparticle/PET nanofiber.

TABLE III
Elastic Moduli of Iron Oxide Nanoparticle/PET Nanofibers

	Elastic modulus (GPa)
5 wt % Fe_3O_4	0.052
10 wt % Fe_3O_4	0.117
15 wt % Fe_3O_4	0.201
5 wt % Fe_3O_4 (0.03 T)	0.070
10 wt % Fe_3O_4 (0.03 T)	0.149
15 wt % Fe_3O_4 (0.03 T)	0.328

consistent with that of the tensile test. When the external magnetic field was applied, the slope of nanoindentation curves becomes steeper. This improvement of the elastic modulus is thought to be due to the dipole-dipole interaction and exchange coupling effect of magnetic nanoparticles.

CONCLUSIONS

Iron oxide nanoparticles with sizes below 25 nm were separated and iron oxide nanoparticle/PET nanowebs were fabricated using electrospinning. The diameter of nanofibers increased with iron oxide nanoparticle concentration because diameter thickening effect due to viscosity increase was dominant to diameter thinning effect caused by increase of Coulomb force. DSC results indicated crystallinity increase of iron oxide nanoparticle/PET nanowebs with iron oxide nanoparticle loading. SQUID measurement confirms that the iron oxide nanoparticle/PET nanofiber shows the superparamagnetic behavior with a small remnant magnetization at zero field. Flexural rigidity and tensile properties of iron oxide nanoparticle/PET nanowebs were improved with the external magnetic field. Also, improvement in the elastic modulus of the magnetic nanofibers was confirmed.

It is expected that the combination of the flexibility of polymeric nanofiber and the superparamagnetic behavior of the iron oxide nanoparticles can be led to the application of field-responsive protection. The follow-up works are in progress to investigate debonding mechanism of iron oxide nanoparticles in PET matrix and to prepare more strong magnetic nanofibers.

This work was supported by DAPA (Defense Acquisition Program Administration) and ADD (Agency for Defense Development, South Korea).

References

1. Epstein, A. J.; Miller, J. S. Synth Met 1996, 80, 231.
2. Pinchuk, L. S.; Markova, L. V.; Gromyko, Y. V.; Markov, E. M. J Mater Process Technol 1995, 55, 345.
3. Alexiou, C.; Arnold, W.; Klein, R. J.; Parak, F. G.; Hulin, P.; Bergemann, C.; Erhardt, W.; Wagenpfeil, S.; Lubbe, A. S. Cancer Res 2000, 60, 6641.
4. Martin, J. I.; Nogues, J.; Liu, K.; Vicent, J. L.; Schuller, I. K. J Magn Magn Mater 2003, 256, 449.
5. Fert, A.; Piraux, L. J Magn Magn Mater 1999, 200, 338.
6. Wu, H.; Zhang, R.; Liu, X. X.; Lin, D. D.; Pan, W. Chem Mater 2007, 19, 3506.
7. Mayes, E. L.; Vollrath, F.; Mann, S. Adv Mater 1998, 10, 801.
8. Wang, B.; Sun, Y.; Wang, H. J App Polym Sci 2010, 115, 1781.
9. Song, T.; Zhang, Y. Z.; Zhou, T. J. J Magn Magn Mater 2006, 303, 286.
10. Wang, M.; Singh, H.; Hatton, T. A.; Rutledge, G. C. Polymer 2004, 45, 5505.
11. Wang, Y. X.; Hussain, S. M.; Krestin, G. P. Eur Radiol 2001, 11, 2319.
12. Bossis, G.; Lacis, S.; Meunier, A.; Volkova, O. J Magn Magn Mater 2002, 252, 224.
13. Feng, L.; Li, S.; Li, H.; Zhai, J.; Song, Y.; Jiang, L.; Zhu, D. Angew Chem Int Ed 2002, 41, 1221.
14. Ma, P. X.; Zhang, R. J Biomed Mat Res 1999, 46, 60.
15. Liu, G. J.; Ding, J. F.; Qiao, L. J.; Guo, A.; Dymov, B. P.; Gleeson, J. T.; Hashimoto, T.; Saijo, K. Chem Eur J 1999, 5, 2740.
16. Reneker, D. H.; Chun, I. S. Nanotechnol 1996, 7, 216.
17. Deitzel, J. M.; Kleinmeyer, J. D.; Hirvonen, J. K.; Beck Tan, N. C. Polymer 2001, 42, 8163.
18. Huang, Z. M.; Zhang, Y. Z.; Kotaki, M.; Ramakrishna, S. Compos Sci Technol 2003, 63, 2223.
19. Gupta, P.; Asmatulu, R.; Claus, R.; Wilkes, G. J Appl Polym Sci 2006, 100, 4935.
20. Ahn, B. W.; Chi, Y. S.; Kang, T. J. J Appl Polym Sci 2008, 110, 405.
21. Lee, S. S. J Appl Polym Sci 2009, 114, 3652.
22. Ye, S. H.; Zhang, D.; Liu, H. Q.; Zhou, J. P. J Appl Polym Sci 2011, 121, 1757.
23. Brandrup, J.; Immergut, E. H.; Grulke, E. A.; Abe, A.; Bloch, D. R. Polymer handbook, 4th ed.; Wiley: New York, 1999.
24. Tan, E. P. S.; Lim, C. T. Compos Sci Technol 2006, 66, 1102.
25. Shin, Y. M.; Hohman, M. M.; Brenner, M. P.; Rutledge, G. C. Appl Phys Lett 2001, 78, 1149.
26. McKee, M. G.; Wilkes, G. L.; Colby, R. H.;Long T. E. Macromolecules 2004, 37, 1760.
27. Barnes, H. A.; Hutton, J. F.; Walters, K. An Introduction to Rheology; Elsevier Science: Amsterdam, 1989.
28. Asano, T.; Calleja, F. J. B.; Flores, A.; Tanigaki, M.; Mina, M. F.; Sawatari, C.; Itagaki, H.; Takahashi, H.; Hatta, I. Polymer 1999, 40, 6475.
29. Klien, C.; Hurlbut, C. S.; Dana, J. D. Manual of Mineralogy, 20th ed.; Wiley: New York, 1985.
30. Mbhele, Z. H.; Salemane, M. G.; van Sittert, C. G. C. E.; Nedeljkovic, J. M.; Djokovic, V.; Luyt, A. S. Chem Mater 2003, 15, 5019.
31. Gedde, U. W. Polymer Physics, 1st ed.; Chapman and Hall: London, 1995.
32. Li, Y.; Huang, Z. M.; Lu, Y. Eur Polym Mater 2006, 42, 1696.
33. Kodama, R. H. J Magn Magn Mater 1999, 200, 359.
34. Kunugi, T.; Ichinose, C.; Suzuki, A. J Appl Polym Sci 1986, 31, 429.
35. Suzuki, A.; Kawada, T. J Appl Polym Sci 2002, 83, 179.
36. Hou, H. Q.; Ge, J. J.; Zeng, J.; Li, Q.; Reneker, D. H.; Greiner, A.; Cheng, S. Z. D. Chem Mater 2005, 17, 967.
37. Zuiderduin, W. C. J.; Westzaan, C.; Huetink, J.; Gaymans, R. J. Polymer 2003, 44, 261.
38. Guild, F. J.; Young, R. J. J Mater Sci 1989, 24, 298.
39. Bossis, G.; Volkova, O.; Lacis, S.; Meunier, A. Ferrofluids magnetically controllable fluids and their applications; Springer: Berlin, 2002.